35th Space Symposium, Technical Track, Colorado Springs, Colorado, United States of America
Presented on April 8, 2019

RENDEZVOUS MISSION RISK REDUCTION THROUGH PASSIVE SAFETY ANALYSIS

McClain M. Goggin
Purdue University, mgoggin@purdue.edu

Dr. David A. Spencer
Purdue University, dspencer@purdue.edu

ABSTRACT

Orbital rendezvous is a critical phase for missions that perform satellite servicing, active debris mitigation, in-space manufacturing, space station resupply, and planetary sample return. One method for reducing risk in orbital rendezvous applications is to design the approach trajectory such that no collision will occur if the ability to maneuver is compromised by a fault. Approaches for passively safe rendezvous design are routinely applied for human and robotic space flight.

A passive safety analysis of a rendezvous mission is used to evaluate the total probability of collision in the event that the maneuvering chaser spacecraft experiences a fault that results in a loss of maneuvering capability. The key factors in determining the passive safety of a rendezvous mission are the chosen approach trajectory, state estimation technique, and probability of collision calculation. This paper will demonstrate how rendezvous mission elements can be designed to achieve a desired level of collision risk using a state covariance approach. A Kalman filter is used to generate an improved relative state estimate and state estimate uncertainty covariance based on a nominal approach trajectory and realistic sensor noise values. The state covariance matrix following each state update is used to predict the probability of collision if a fault were to occur at that time. The effectiveness of this approach for designing passively safe terminal rendezvous trajectories is demonstrated through a set of case studies of rendezvous scenarios. These case studies emphasize that total rendezvous collision probability is reduced by reducing the time spent on collision or near collision trajectories.

INTRODUCTION

Orbital rendezvous and proximity operations have been an important means of accomplishing mission objectives since the start of the space age[1]. During the 1960s and 70s, both the United States and the Soviet Union considered orbital rendezvous a key enabling technology[2] for space exploration. Orbital rendezvous enabled humans to get to the moon, assemble and supply space stations, and repair the Hubble space telescope. While dozens of vehicles have flown rendezvous missions to date, there are far more rendezvous mission concepts currently being developed by entities ranging from government agencies and universities to large corporations and small startups. These concepts include satellite servicing, orbital debris removal, in-space manufacturing, space station re-supply, and planetary science sample return missions. These missions will have to decide what level of risk is acceptable, and what steps they can take to reduce the risk.

Orbital rendezvous represents a critical event that involves significant operational complexity which in turn increases mission risk. This operational complexity drives visiting vehicles to the International Space Station to be overseen by astronauts in orbit, teams at NASA Johnson Space Center, and the mission operations center of the vehicle[3] during rendezvous and berthing. Despite numerous precautions to reduce mission risk, several orbital rendezvous failures are documented. In 1997, an unmanned Russian Progress resupply vehicle collided with the Mir space station forcing astronauts onboard to seal off sections of the station[4]. That same year, the ETS-VII rendezvous and docking demonstration vehicle experienced multiple anomalies during the final phases of rendezvous[5]. In 2005, DARPA's Demonstration of Autonomous Rendezvous Technology (DART) mission experienced a fault that resulted in a collision[6,7]. These mishaps still affect perceptions about the risks of rendezvous missions to this day.

The probability that a given rendezvous mission design results in an uncontrolled collision is influenced by numerous design decisions ranging from approach trajectory to navigation filter methodology to sensor selection and hardware reliability. As the number of rendezvous missions increases, designers may wish to impose a maximum acceptable probability of uncontrolled collision as a design requirement. Program managers may wish to see how this indicator of mission risk is impacted by design decisions, and weigh them against the related cost implications. Engineers will inevitably want to design an optimal rendezvous for their specific missions. The purpose of this paper is to provide a framework that can be used to evaluate the probability of collision due to loss of maneuverability during the terminal rendezvous phase of a mission.

While orbital rendezvous can enable many different missions, this paper investigates the design of a Mars sample return scenario involving the capture of an orbiting sample canister (OS) by an Earth return orbiter (ERO). In this scenario, the one-way light time between Mars and Earth prohibits ground-in-the-loop control of the rendezvous. The absence of GPS and ground-based target tracking around Mars results in the need for an automated rendezvous using the ERO proximity sensor suite for relative state estimation. A rendezvous around Mars is therefore an ideal candidate for a passively safe approach. As with Berger[8], a passively safe trajectory has been defined as an approach trajectory in which the probability of collision is negligible, even without the use of thrusters. In the event of a fault caused by an extended period during which the OS is not visible to the ERO, it would be advantageous for the ERO to be on a low probability of collision trajectory in order to allow the vehicle to passively wait to reacquire visibility of the OS without using additional fuel. The same passively safe trajectory would allow the ERO to completely shut off its thrusters in the event of a more serious fault.

This paper provides a method for evaluating the probability of collision for a rendezvous mission by integrating trajectory design, relative state estimation, and probability of collision calculations based on passive safety. Evaluating the probability of collision of rendezvous mission concepts provides four immediate and important applications. First, the method can be used to evaluate or compare mission design concepts based on probability of collision. Second, the method can be used to create hardware reliability requirements for missions. Third, the method can provide stakeholders with an indication of mission risk. Finally, the method can provide onboard fault protection systems with the information needed to determine the appropriate response in the event of a fault during the rendezvous phase. This paper focuses on the application of this method to a trade study between trajectory design parameters and the total collision probability for the mars sample return mission.

Literature Review

Factors affecting the probability of collision for a rendezvous mission can be grouped into three main categories, each of which have individually been the subject of extensive research. The first category consists of the rendezvous dynamics and approach strategies, the second consists of relative state estimation methods, and the third consists of collision probability determination methods.

Rendezvous Dynamics and Approach Trajectories

The rendezvous phase involves the relative motion of a maneuvering "deputy" spacecraft with respect to a non-maneuvering "chief". This relative motion is commonly described in the local vertical local horizontal (LVLH) reference frame centered on the chief vehicle. It consists of the chief radius vector, the chief orbital angular momentum vector, and the vector that completes the right-handed triad in the direction of motion.

Extensive work has been done by Scharf et al.[9], Alfriend and Yan[10], and Sullivan et al.[11] to compile the closed form relative dynamics models currently available. These models range from the well-known linear translational model of Clohessy-Wiltshire (CW) that has seen extensive flight heritage[11] and their extension to curvilinear coordinates by Alfriend et al.[12] and De Bruijin et al. [13], to the orbital element state representation models by Schuab[14], Yan [15], and Vallado[16]. The simplest dynamics models involve assumptions such as a circular chief orbit and small spacecraft separation. From these basic relative dynamics models, extensions are made to include either larger spacecraft separations, chief eccentricity[17], perturbations[18,19], or some combination thereof[12].

In Fehse's discussion of rendezvous trajectory types[20], he details ten transfer types for rendezvous with vehicles in near-circular orbits. He groups them into radial impulse transfers, tangential impulse transfers, and straight-line trajectory transfers. One common rendezvous approach is to combine a radial impulse transfer and a straight-line transfer with constant velocity. This is a commonly used two-phase approach strategy[1] because the initial portion takes advantage of natural dynamics to introduce some level of passive safety[21] while the final portion overcomes the relative dynamics using thrusters to increases the level of control for a successful docking/mating. Each impulse during a rendezvous will incur maneuver execution errors which may be modeled as a combination of magnitude and pointing errors that are proportional to the applied impulse [22]. These errors are important because they increase relative state uncertainty and can alter the initially planned trajectory.

Relative State Estimation

While there are many methods for observing the relative state, all the techniques are susceptible to noise. To produce an improved relative state estimate, the noisy observations are passed through a state estimation filter. One of the important aspects of any state estimation filter is the resulting variance-covariance matrix. This matrix defines a hyper-ellipsoid of the distribution of potential positions and velocities, and an ellipsoid describing the potential positions. This position ellipsoid has a surface with constant probability density[23] and provides a visual representation of where the true relative position is the most likely to be.

The two most common filters used in orbit determination are least squares and sequential processing filters[24]. Least squares filters are ideally suited for quickly obtaining a state estimate from large quantities of data, while sequential processing methods are best suited for improving upon a previous state estimate in real-time while describing the potential error in the state with a covariance matrix. The Kalman filter[25] and its extensions are probably the best known sequential filters and have been extensively used to improve state estimates of dynamic systems from noisy observation data. The Extended Kalman Filter (EKF) is simply the extension of the linear Kalman filter to nonlinear dynamics. As noted by Sullivan[26] the EKF still requires a first order linearization to propagate the state uncertainty covariance. The Unscented Kalman Filter (UKF) as developed by Julier[27] enables the state uncertainty covariance to be propagated using nonlinear dynamics by generating a representative set of weighted points and propagating them through the nonlinear dynamics. The weights ensure that the state estimate is the mean of the distribution of points both before and after the propagation. The Kalman filter and its extensions are especially suited to the rendezvous problem because they continually update the relative state and covariance as new relative observations are taken.

Collision Probability

There are two main methods for determining collision probability. The first is through covariance analysis and is the focus of this research. The second is through Monte Carlo analysis which is considered more accurate[28] but is also far more time and resource intensive. . A Monte Carlo analysis generates a statistically significant number of potential initial states, propagates them individually, and uses the percent of the initial states that result in a collision as the collision probability.

Covariance analysis uses the assumption that the relative state uncertainty follows a Gaussian distribution, and the probability that the true state is located at a given location can be determined by a Gaussian probability density function. Th collision probability at a single instant in time is determined as the probability that the center of mass of the deputy vehicle lies within the volume of a sphere created by adding together the maximum radius of each spacecraft. Any relative states within this “combined hardbody” are considered to have collided. The biggest limitation in the accuracy of covariance analysis in determining the probability of collision is the presence of any unmodeled dynamics when propagating the covariance matrix. When model used to propagate the covariance is accurate, the accuracy of covariance probability analysis increases

Methods for calculating collision probability from a state covariance depend on the amount of time the spacecraft spend in close proximity to one another. In his book on spacecraft collision probability Chan[29] categorizes spacecraft collision probability methods based on the relative velocity of the spacecraft. For most orbital spacecraft encounters not involving rendezvous, the relative velocity is high and encounters last only a few seconds. These high velocity encounters are typically modeled as rectilinear motion. There are many methods of calculating collision probabilities for the rectilinear case, however none of them can be directly applied to the low velocity case of a rendezvous where the motion of one spacecraft with respect to another does not resemble a straight line.

Phillips [30] compiled an extensive review and comparison of extended encounter collision probability methods. These methods range from the development of an analytic solution that must be rederived for any given relative orbit geometry from Chan[29], to methods that break the relative trajectory into small increments of near rectilinear motion that can be combined to generate a total probability of collision such as that by Patera[31], and McKinley [32]. These methods convert reference frames to a constant covariance centered at the origin of the LVLH frame. They then have the combined hardbody change size and shape with time to create a single, time-invariant volume representing the entire trajectory. The methods then integrate the probability density function over this time-invariant volume swept out by the time-varying shape of the combined hardbody. This volume integral is typically very small while the deputy vehicle is near its initial condition, but grows as the deputy approaches the chief, and as the covariance expands with time. In the case of a rendezvous where the deputy range is decreasing while the covariance is expanding, the probability of collision is almost entirely contained within a small portion of the swept-out volume. One useful method for approximating this integral, and thereby saving substantial computation time, is by taking the instantaneous collision probability as determined by a single covariance at the time of maximum collision probability.

EVALUATING RENDEZVOUS COLLISION PROBABILITY

The total collision probability for a rendezvous mission is determined by the trajectory design and dynamics models used, the state estimation methodology employed, and the way in which the collision probability is calculated. Exhibit 1 shows how trajectory design, state estimation, and collision probability determination affect the final collision probability. The trajectory design provides the relative state (x) and planned maneuvers ($\Delta\bar{V}$) using the state estimate ($\hat{x}$) determined by the filter. The relative position is then observed (z) using onboard state determination sensors that are simulated by adding Gaussian white noise to the true relative state, and the filter improves upon these observations. The state estimate ($\hat{x}$) and state uncertainty covariance (C) are then used to determine the probability that a collision will occur (P_{ct}) if a fault occurs (with a probability of occurring P_F) at the time of the observation (t). The total collision probability (P_T) of the terminal rendezvous phase of the mission is then determined by taking 1 minus the probability that no collision occurred as described in equation 12. The probability that no collision occurred includes both the probability that no faults occurred and that any faults that did occur did not result in a collision.

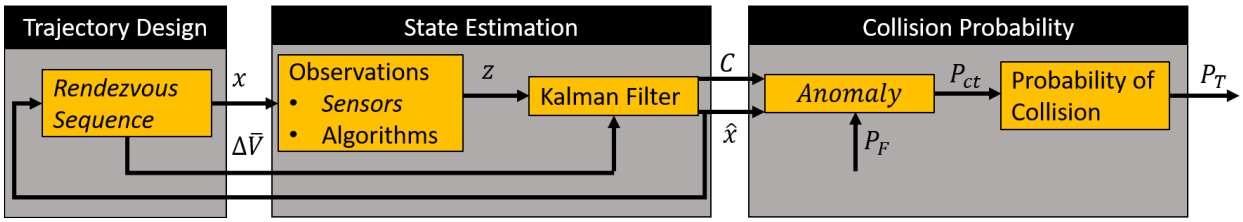

Exhibit 1: Information process flow for calculating rendezvous collision probability

The rendezvous trajectory maneuvers were planned by solving for the desired impulse using the linearized CW equations and relative orbital elements (ROEs) as defined by Lovell and Tragesser[33]. Planning maneuvers based on

ROEs requires that the assumptions under which the ROEs were defined are valid for the mission being evaluated. The analysis presented in this paper evaluates a rendezvous mission between a maneuvering ERO (deputy) and a non-maneuvering OS (chief) around Mars. It is assumed that the OS is in a low inclination, 480 km circular orbit, and initial conditions were chosen that place the ERO in a co-orbital hold point 50 meters ahead of the OS in preparation for terminal rendezvous. This small separation distance and circular reference orbit result in very little deviation from the motion described by CW equations, while the low inclination 480 km altitude result in minimal perturbations due to the J2 spherical harmonic and drag perturbations.

Simulations were run using both a high fidelity model with inertial propagation, J2 perturbations, and an unscented Kalman filter as described by Julier[27], and a much faster simplified model using CW propagation and a linear Kalman filter. The simplified model was used to generate numerous cases in parameter trade studies while the high-fidelity model was used to evaluate individual cases and to verify the results of the simplified model.

Collision Probability

Both the high-fidelity model and the simplified model use the same method for collision probability estimation. At each new state observation, the collision probability estimator propagates the best estimate of the relative state and state uncertainty covariance through one full orbit or revolution (rev) from the time of the observation and determines the probability that a fault occurring following that state observation and before the next observation would result in a collision trajectory (P_{ct}). This provides one rev advanced notice on the probability of collision. In the event of a fault, the collision probability would continue to be extended in order to determine if an active or passive abort were required. The collision probability estimation method does this by linearly propagating three different indicators of collision probability through one rev and finding the point of maximum indicated collision probability. The maximum of these instantaneous collision probabilities is then used to represent the collision probability of a fault occurring at that time.

Closest approach indicators

A single initial state can be propagated forward in time to determine if it will result in a collision. Similarly, a distribution of initial states can be propagated forward in time to determine what percent of the original distribution will result in a collision, as is done in Monte-Carlo analysis. A state uncertainty covariance matrix describes a distribution of initial states and can be propagated forward in time to describe what percent of the original distribution will result in a collision without requiring the propagation of a significant number of individual initial states.

If a covariance represents the potential distribution of relative states at a given time, propagating this covariance with time shows the potential distribution of trajectories. The left side of Exhibit 2 shows a planar view in the LVLH frame of a set of three trajectories propagated through ¾ of a rev beginning at 10 meters, 15 meters, and 20 meters from the combined hardbody centered at the origin. Each trajectory is propagated for one rev and is denoted by the red "nominal" arc. Each exhibit also shows the corresponding distribution of points as described by the 3σ covariance ellipsoid at two-minute intervals along the trajectory. The 3σ[low] arc shows the potential path of one initial state on the "lower" boundary of the initial covariance. The 3σ[high] arc shows the potential path of a different initial state on the "high" boundary of the initial covariance. Looking at the intersection of these and other potential trajectories with the combined hardbody radius shows that the time when the most potential trajectories are collision trajectories is represented by a single 3σ covariance ellipsoid. Evaluating a single collision probability integral using this approximation can dramatically reduce computation time. This reduction in computation time is important because the relative state estimate and state estimate covariance will change with every new observation so the probability of collision must also be re-determined with each observation.

The question then becomes how to identify when to calculate the instantaneous collision probability such that it is representative of the likelihood that a collision will occur if an anomaly occurs that prevents future maneuvers

from being implemented. For rectilinear motion when relative velocities are high, the location of closest approach is used to calculate the instantaneous collision probability. For trajectories with low relative velocities this is no longer the case because relatively small variations in trajectories can lead to significantly different locations of maximum collision probability.

The right side of Exhibit 2 shows how the instantaneous collision probability varies for the trajectory shown on the left throughout one full rev. The beginning of the trajectory is marked by the red dot. As the trajectory progresses, the state uncertainty grows as the nominal range from the origin decreases. For the ten-meter case, the trajectory results in an almost 100% of all potential trajectories result in a collision with the combined hardbody. However, every instant along the trajectory does not correspond to a 100% probability of collision. In fact, the point at which the nominal trajectory passes through the origin, the instantaneous collision probability is not 100% because the 3σ state uncertainty covariance extends beyond the hardbody. As the initial trajectory location is changed to 15 and 20 meters, the location where the maximum collision probability occurs changes. An indicator that considers both the size of the covariance and the nominal range must be used to determine where the instantaneous collision probability should be calculated.

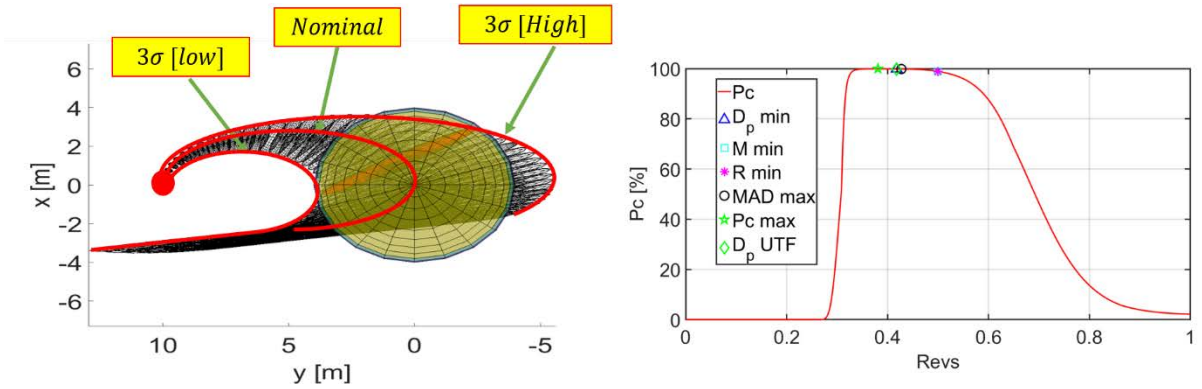

Exhibit 2a: The 10-meter case

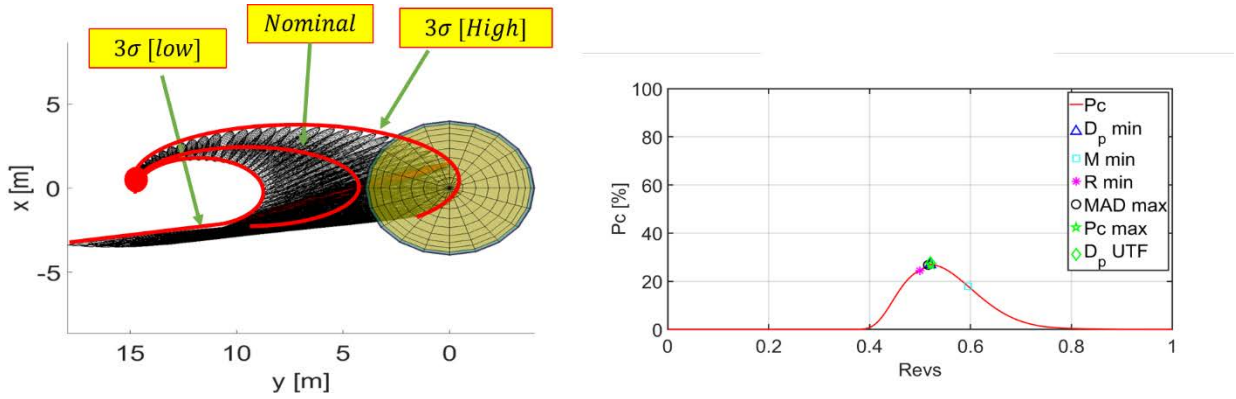

Exhibit 2b: The 15-meter case

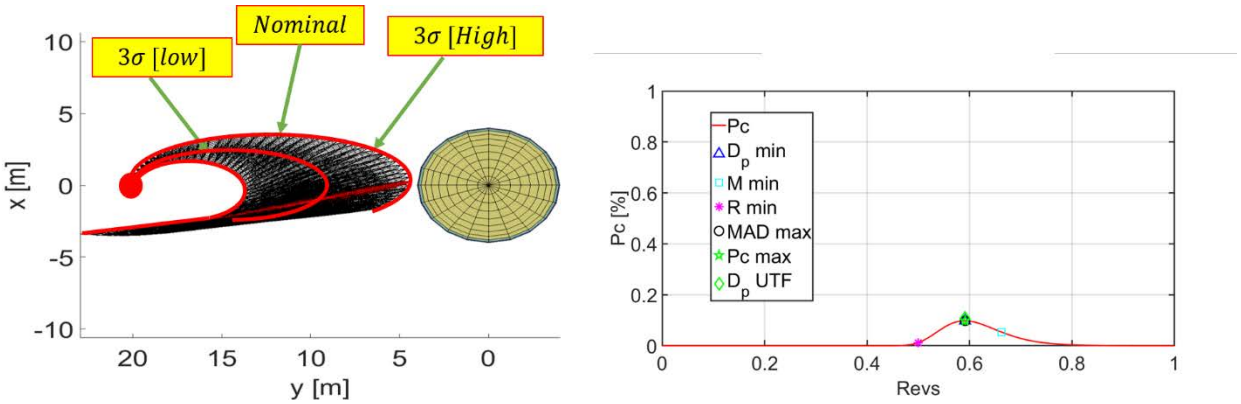

Exhibit 2c: the 20-meter case

Exhibit 2: Example trajectories beginning at ranges of10m, 15m, and 20m showing the growth of the covariance through the trajectory and where the covariance intersects with the combined hardbody. Also shown is the corresponding instantaneous collision probability and collision probability indicators.

Three indicators were identified for approximating the location of maximum probability of collision: The minimum projection distance, the minimum Mahalanobis distance, and an maximum approximation of the collision probability using the Method of Approximated Distribution[29]. The projection distance scales the range at every point along the trajectory by the projection of the probability density function described by the covariance along the relative position vector

$$D_{p|min} = \min \frac{||\hat{\rho}||}{\hat{r} C_r \hat{r}^T} \quad 1$$

where $\hat{\rho}$ is the estimated relative position, $\hat{r}$ is the estimated relative position unit vector, and C_r is the position relative state covariance.

The second indicator is the minimum Mahalanobis distance which is the number of standard deviations a point is from the nominal position[34].

$$M_{min} = \min||\hat{\rho}||\hat{r} C_r^{-1} \hat{r}^T \quad 2$$

The third indicator consists of applying the method of approximating distributions as described by Chan[29] to approximate the instantaneous collision probability integral at given intervals along the estimated trajectory. A full description of this method can be found in reference [29]. The general concept revolves around converting the collision probability integral into a cumulative central chi-square distribution and then converting to a cumulative Gaussian distribution of one variable

$$\mu = \sum_{j=1}^{3} [\sigma_j^2 + \rho_j^2] \quad 3$$

$$\mu_2 = 2 \sum_{j=1}^{3} [\sigma_j^4 + 2\sigma_j^2 \rho_j^2] \quad 4$$

$$\mu_3 = 8 \sum_{j=1}^{3} [\sigma_j^6 + 3\sigma_j^4 \rho_j^2] \quad 5$$

$$n' = \frac{8\mu_2^3}{\mu_3^2} \quad 6$$

$$X^2 = n' + \sqrt{\frac{2n'}{\mu_2}}\,(R^2 - \mu) \quad (7)$$

$$T = \left[\sqrt[3]{\frac{X^2}{n'}} - \left(1 - \frac{2}{9n'}\right)\right] \Big/ \sqrt{\frac{2}{9n'}} \quad (8)$$

$$P_{MAD} = \frac{1}{2}\left[1 + \operatorname{erf}\left(\frac{T}{\sqrt{2}}\right)\right] \quad (9)$$

where ρ_j is the relative position element of the relative position vector $\bar{\rho} = [\rho_1, \rho_2, \rho_3]$, σ is the diagonal element of the position uncertainty covariance (C_r) and R is the combined hardbody radius. This approximation typically indicates and agrees with the maximum collision probability location and value. However, it encounters limitations when the covariance is substantially larger on one axis than the others. This limitation introduces the need to perform checks using another indicator.

The locations determined by the minimum projection distance(D_p), minimum Mahalanobis distance (M), and the point of the maximum collision probability using the method of approximate distributions (MAD) have been shown on the right column of Exhibit 2 and the corresponding maximum collision probability covariance ellipsoid has been highlighted in red in the left column of the Exhibit. Once the location of maximum collision probability is determined, the unscented transform (UTF) is used to propagate the state and covariance through nonlinear dynamics and the collision probability is reevaluated.

Instantaneous Probability of Collision

If the center of mass of the ERO is closer to the origin than the combined hardbody radius (CHR), a collision is assumed to occur because that is where the two spheres describing the individual hardbodies would intersect. At any instant in time, the uncertainty in the relative position of the center of mass of the ERO with respect to the OS is described by a covariance matrix. For a Gaussian uncertainty distribution, the probability density function in the form of equation 10 describes the probability that the center of mass of the ERO lies within the volume of a sphere of their combined hardbody radius[30]

If the center of mass of the ERO is closer to the origin than the combined hardbody radius (CHR), a collision is assumed to occur because that is where the two spheres describing the individual hardbodies would intersect. At any instant in time, the uncertainty in the relative position of the center of mass of the ERO with respect to the OS is described by a covariance matrix. For a Gaussian uncertainty distribution, the probability density function in the form of equation 10 describes the probability that the center of mass of the ERO lies within the volume of a sphere of their combined hardbody radius[30]

$$P\ \frac{1}{\sqrt{(2\pi)^3|C_r|}} \iiint e^{\frac{1}{2}\bar{x}^T C^{-1} \bar{x}}\, dxdydz \quad (10)$$

where $|C|$ is the determinant of the position covariance matrix and $\bar{x}$ is the volume integration parameter. This integral can be numerically integrated or approximated using one of several approaches including the method of approximate distributions described in equations 3-9.

Total collision probability

During a rendezvous mission, the relative state is being constantly updated to produce a new estimated state and state uncertainty covariance. Based on sensor inputs, additional state estimations generally reduce the

trajectory uncertainty. For a passively safe trajectory, the collision probability will decrease as the ERO moves along the trajectory taking in new relative state observations. For a non-passively safe trajectory, the collision probability may increase as it moves along the trajectory acquiring new state observations. For trajectories that loop back on themselves, the collision probability first decreases as an improved state estimate is acquired, then increase as the probability of collision due to a fault that lasts for a full rev becomes significant.

If a fault occurs during the rendezvous sequence, it is assumed that future maneuvers during the approach phase cannot be performed. The total collision probability calculation must therefore include the probability that a fault occurs following any observation time. The probability tree in Exhibit 3 show a graphical representation of how the total collision probability is calculated. The initial node on the top left indicates the vehicle at time T_1, where a sensor input state observation occurs. The probability that a fault occurs at this time is denoted by P_F. If a fault does occur at T_1, the probability that a collision will result from the uncontrolled trajectory is equal to the instantaneous probability of collision at time T_1, $P_C(T_1)$. The combined probability of impact occurring due to a fault at T_1 is equal to the probability of a fault occurring P_F multiplied with the instantaneous probability of collision at T1, $P_C(T_1)$. This combined probability is denoted by P_{ct}^1. Exhibit 3 indicates a series of timesteps, with a node at each time of sensor input. The resulting total collision probability is stated in Equation 12, below.

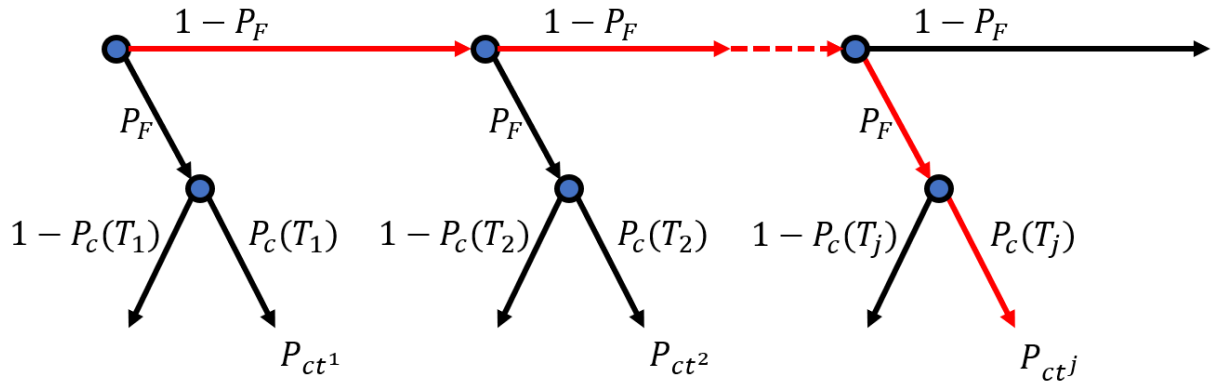

Exhibit 3: Collision probability tree highlighting an example fault at time t^j

In Exhibit 3, P_F is the probability of a fault occurring, $P_c(T_j)$ is the probability that the trajectory following the fault is a collision trajectory and P_{ct^j} is the probability that a fault at time t^j results in a collision. The probability of collision at any time t^j is given by equation 11

$$P_{ct^j} = P_F P_c(T_j)(1 - P_F)^{j-1} \quad 11$$

The total collision probability for the rendezvous sequence is given by 1 minus the probability that a collision occurred due to a fault. This includes both the probability of no anomalies occurring and of passive aborts occurring and is described by equation 12

$$P_T = 1 = \prod_{j=1}^{n}(1 - P_{ct^j}) \quad 12$$

Where P_T is the total collision probability for a given rendezvous sequence, and n is the number of relative state observations performed between the initial maneuver in the rendezvous sequence and the point at which the range estimate is less than the combined hardbody radius.

CASE STUDY RESULTS

Two Mars sample return cases rendezvous scenarios were used as case studies for passive safety evaluation. Both cases involved a stationary hold at +50 meters along the V-bar for a half rev to allow the filter to converge before maneuvers began. The probability of collision calculations begin immediately following this hold. The common parameters for both cases can be found in Exhibit 4.

OS orbit altitude	479 km
OS orbit eccentricity	0
OS orbit inclination	0°
Initial relative position (+y position)	+50 m
State observation noise variance per axis	0.1 m
Maneuver magnitude Error	1.5 %
Maneuver pointing error	1.5 %

Exhibit 4: Baseline rendezvous case parameters

The first case is a ballistic trajectory initiated from a radial impulse. Exhibit 5 shows the trajectory as determined by using the simplified model with CW propagation assuming no maneuver execution error, and the trajectory propagated using the high fidelity (HIFI) model using nonlinear dynamics including the J2 spherical harmonic perturbation and 1.5% maneuver execution error in both magnitude and pointing. The trajectories demonstrate that for the ballistic trajectory, there is very little difference between the simplified model and the HIFI model. Both trajectories assumed an impulsive covariance expansion at the maneuver corresponding to 1.5% expected error.

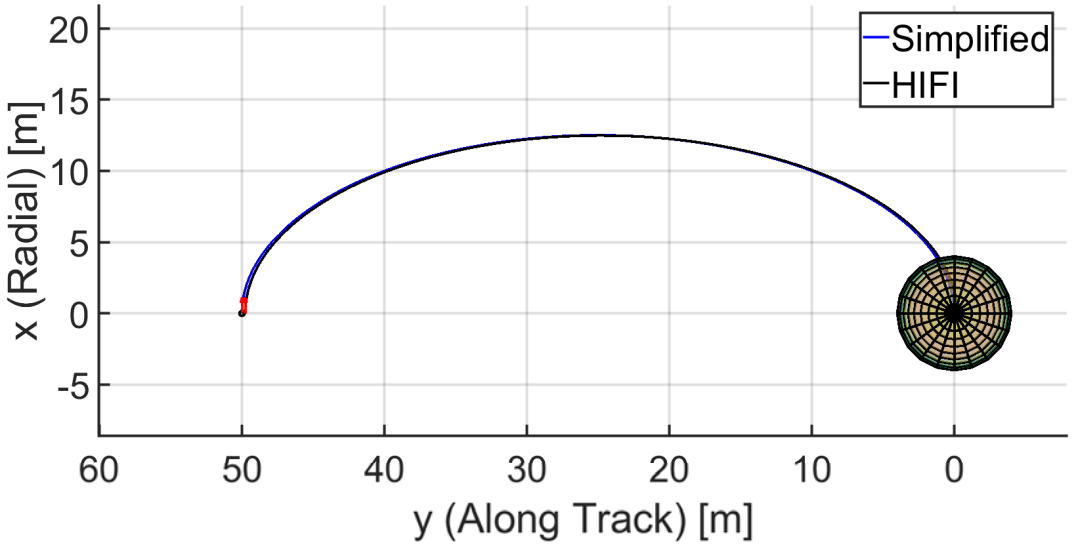

Exhibit 5: Ballistic trajectory showing trajectories propagated using HIFI and simplified model propagation along with the sphere representing the combined hardbody.

Exhibit 6 shows the instantaneous probability of collision calculated at each new observation. Within 0.05 revs, of the start of the rendezvous sequence following the initial hold, the filter converges sufficiently to predict a 100 percent probability of collision. Exhibit 6 shows that from the moment the single hop transfer begins until a successful dock has occurred, the spacecraft is on a collision trajectory. This exhibit shows that no part of this trajectory is passively safe. This ability to predict the that the spacecraft is on a collision trajectory in real time is of

significant interest when designing fault protection strategies. Engineers and project sponsors can set collision probability thresholds above which an active abort should be performed, and under which a passive abort should be executed.

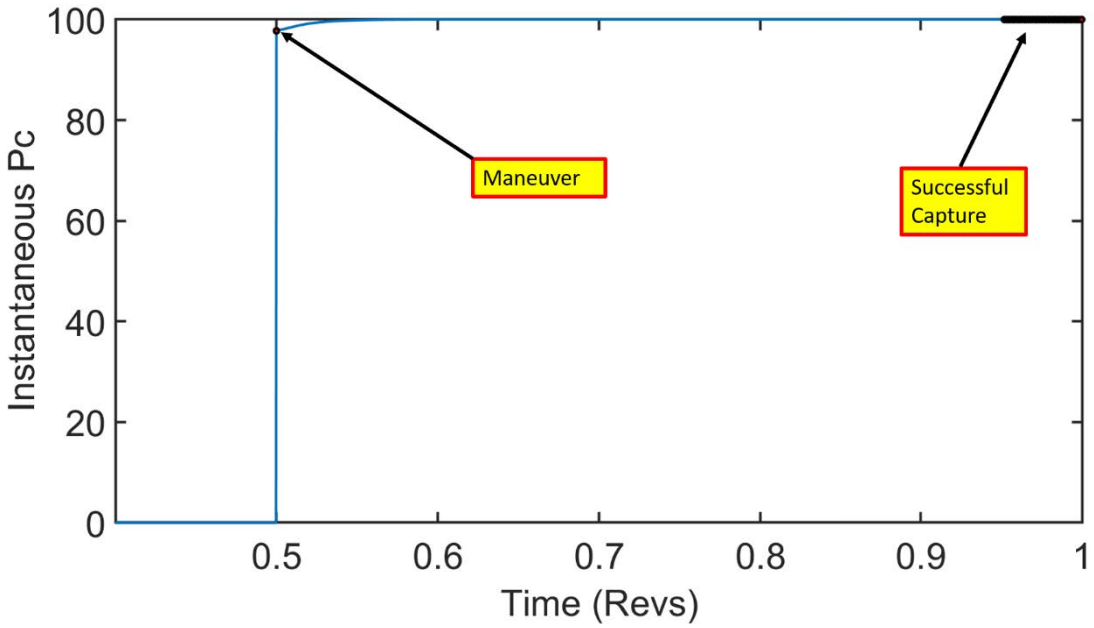

Exhibit 6: Estimated maximum instantaneous probability of collision calculated at each relative state observation for a ballistic trajectory, where the rendezvous sequence following the hold begins after 0.5 revs.

Exhibit 7 shows the effect of breaking up the trajectory into smaller V-bar hops. Increasing the number of hops initially decreases the total probability of a collision following a fault because while each hop takes the same amount of time, the time until a successful capture on the final hop decreases due to the larger percent of the hop that is taken up by the combined hardbody sphere. A successful capture was defined by the point at which the estimated range is less than the CHR. As the hops continue to get smaller however, entire hops occur in the vicinity of the OS without a successful capture. Because each hop takes the same amount of time regardless of size, the covariance expands the same amount during each hop. When this covariance expansion occurs near the OS, the collision probability increases despite the portion of the final hop occupied by a successful capture continuing to decrease.

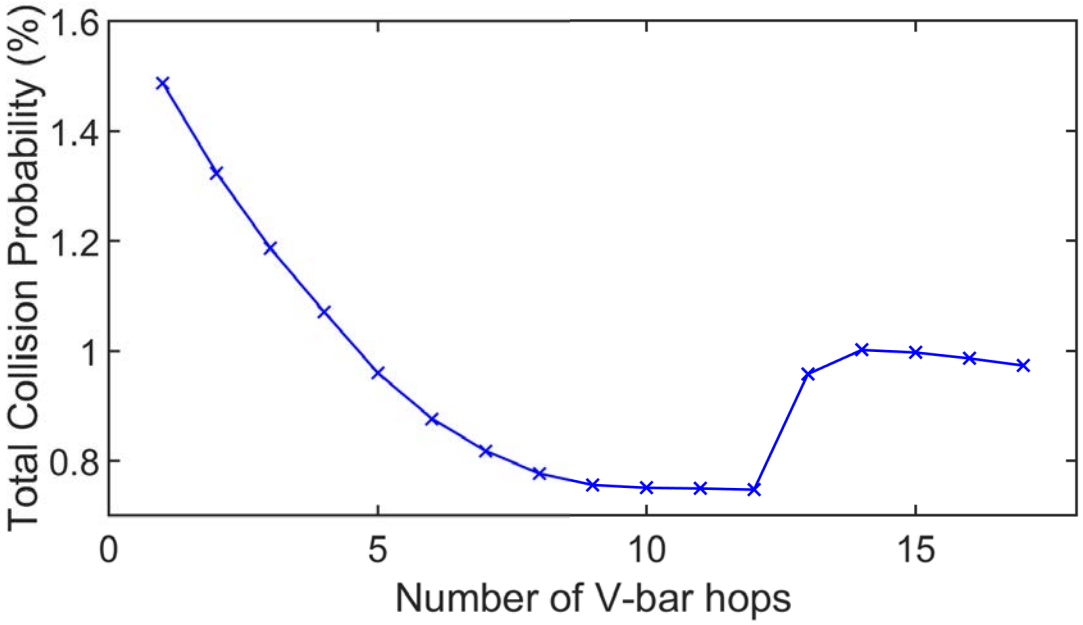

Exhibit 7: Total rendezvous collision probability for increasing number of V-bar hops showing both the case where the probability of a fault occurring at a maneuver is equal to, and ten times larger than, the probability of a fault occurring at any other time.

The second case that was evaluated was a two-phase rendezvous consisting of four initial V-bar hops followed by a straight-line V-bar approach. This trajectory can be seen for both the simplified model and the high-fidelity model in Exhibit 8.

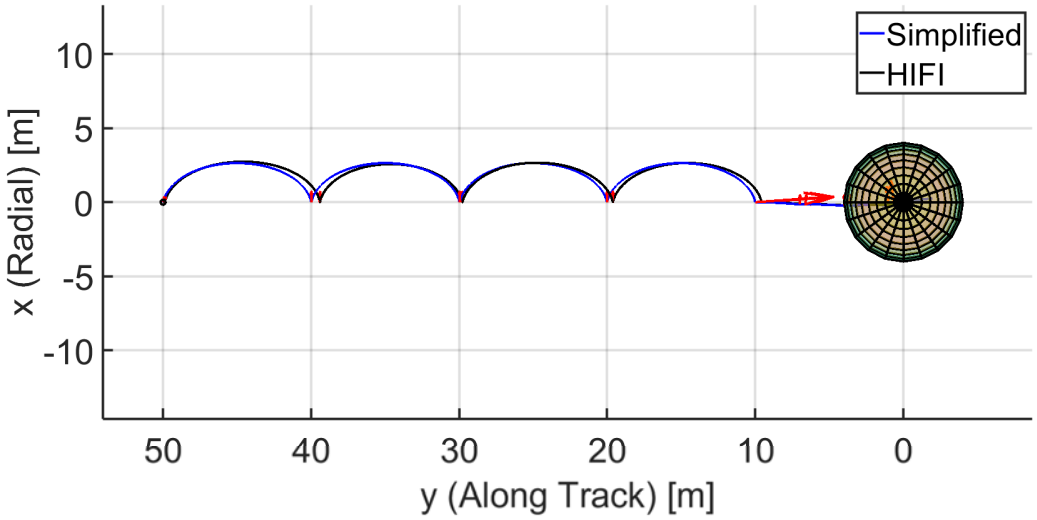

Exhibit 8: Trajectory showing four V-bar hops followed by a straight-line approach for trajectories propagated using HIFI and simplified model propagation with the sphere representing the combined hardbody.

Exhibit 9 shows that the instantaneous probability of collision jumps from essentially zero to one at the transition point between the V-bar hops and straight-line approach due to the reduced time for the covariance to expand with the faster approach than in the case of the additional hop shown previously. The time between this transition point and the point at which the OS is successfully captured however is also reduced substantially. This reduction in the amount of time spent on a collision trajectory reduces the total collision probability from 1.5% in the ballistic trajectory to 0.08% in the two-phase trajectory.

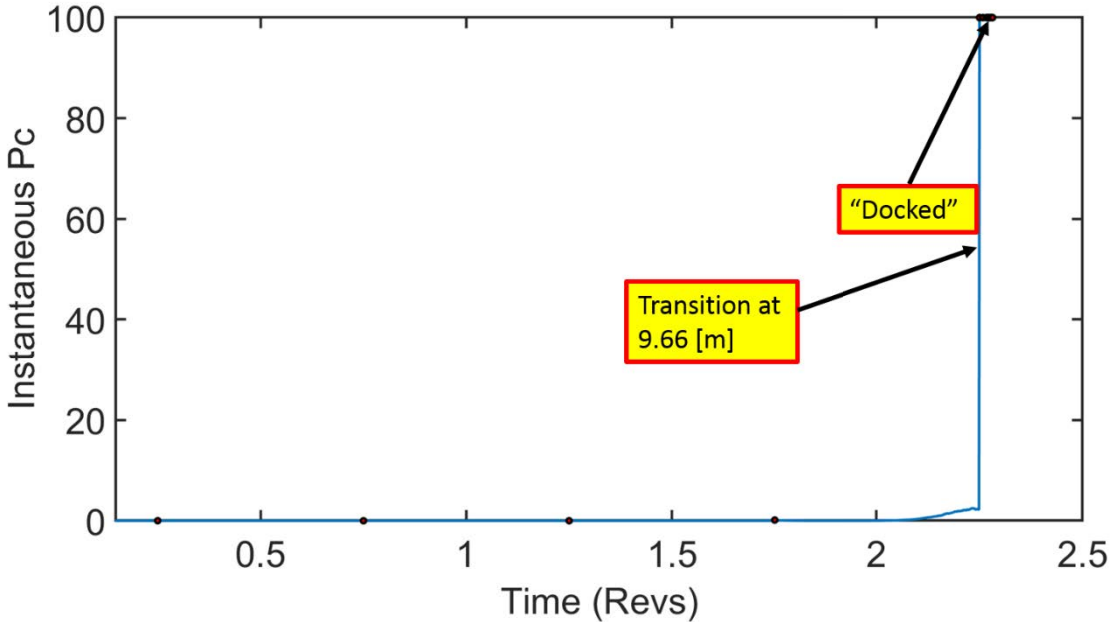

Exhibit 9: Estimated maximum instantaneous probability of collision calculated at each relative state observation for a trajectory with four V-bar hops followed by a straight-line approach.

Exhibit 10 shows the effects of changing the transition point from V-bar hops to a straight-line approach. Exhibit 10 shows that the total probability of collision is relatively constant for the transition to straight-line approach occuring at a range of greater than 10 m. If the transition to a straight-line approach occurs at a range of less than 10 m, the total probability of collision increases.

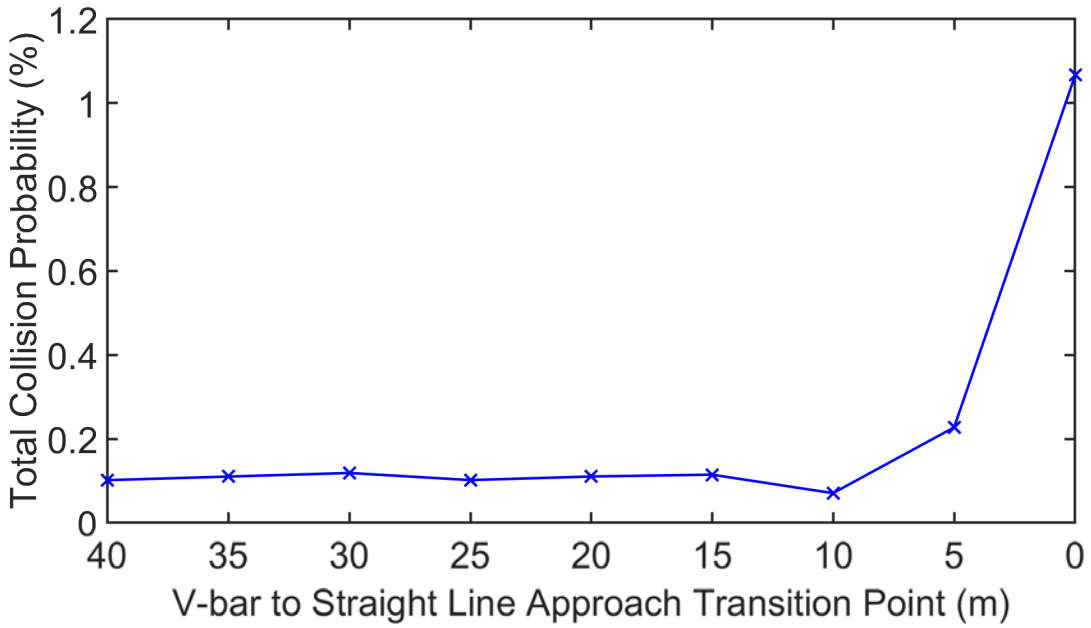

Exhibit 10: Total rendezvous collision probability as a function of the transition point from four V-bar hops to a straight-line approach.

Focusing in on the transition points around 10 meters from the OS, where the total collision probability begins to drop slightly before increasing steeply Exhibit 11 shows that there is a very small minimum collision probability when the transition point is around 8 meters.

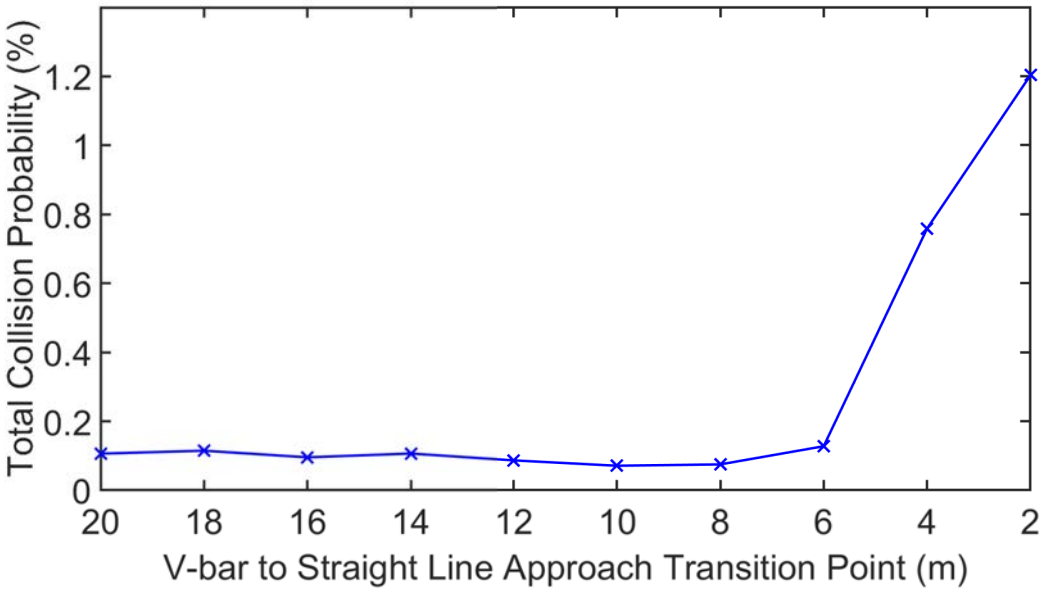

Exhibit 11: Total rendezvous collision probability as a function of the transition point from four V-bar hops to a straight-line approach.

The primary conclusion from these trade studies is that it is possible to provide justification for design decisions based upon an assessment of collision probability. The intuitive result that surfaces from the trade studies performed is that increasing the time spent in close proximity to the OS before completion of the rendezvous sequence increases the total probability of uncontrolled collision. When increasing the number of hops to complete a trajectory as in Exhibit 7, this was accomplished by reducing the size of the final hop, and thereby increasing the portion of the hop that was taken up by a successful capture. Switching to a straight-line transfer or two phase approach reduces the time spent in close proximity to the OS by increasing the horizontal transfer velocity with controlled thrusts.

CONCLUSIONS

As the number of rendezvous missions increases, so too does the need for a framework for evaluating rendezvous mission risk. For a rendezvous sequence, collision probability is perhaps the most intuitive indicator of mission risk. The modular framework presented in this work allows engineers and stakeholders to directly see the impact of design decisions on this important metric. The probability of collision of a rendezvous sequence can be used to justify decisions that would previously have been made based solely upon engineering judgment. This evaluation technique will allow mission designers to characterize the risk associated with the rendezvous phase and establish a maneuver sequence that minimizes the duration during which the approach trajectory is not passively safe. This design method is generally applicable to automated rendezvous and docking and has been used to specifically evaluate the Mars Sample Return scenarios for terminal rendezvous.

---

1. Woffinden DC, Geller DK. Navigating the Road to Autonomous Orbital Rendezvous. *J Spacecr Rockets*. 2007;44(4):898-909. doi:10.2514/1.30734.
2. Polites ME. Technology of Automated Rendezvous and Capture in Space. *J Spacecr Rockets*. 1999;36(2):280-291. doi:10.2514/2.3443.
3. Dempsey RC, Contella DE, Korth DH, et al. Day in the Life: Vital Visiting Vehicles - Keeping the Remote Outpost Crewed and Operating. In: *The International Space Station: Operating an Outpost in the New Frontier*. National Aeronautics and Space Administration; 2017:233-246.
4. Burrough B. *Dragonfly--NASA and the Crisis Aboard MIR*. (Donahue S, ed.). New York: Harper Collins; 1999.
5. Oda M. ETS-VII: Achievements, troubles, and future. *Proc 6th Int Symp …*. 2001:1-7. http://robotics.estec.esa.int/i-SAIRAS/isairas2001/papers/Paper_AS003.pdf.
6. NASA. Overview of the DART Mishap Investigation Results. *Defense*. 2006:1-10. https://www.nasa.gov/pdf/148072main_DART_mishap_overview.pdf.
7. Rumford TE. Demonstration of autonomous rendezvous technology (DART) project summary. In: *SPIE 5088, Space Systems Technology and Operations*. ; 2003:10-19. doi:10.1117/12.498811.
8. Breger L, How JP. Safe Trajectories for Autonomous Rendezvous of Spacecraft. *J Guid Control Dyn*. 2008;31(5):1478-1489. doi:10.2514/1.29590.
9. Scharf DP, Hadaegh FY, Ploen SR. A survey of spacecraft formation flying guidance and control. Part II: control. In: ; 2018. doi:10.23919/acc.2004.1384365.
10. Alfriend KT, Yan H. Evaluation and Comparison of Relative Motion Theories. *J Guid Control Dyn*. 2008. doi:10.2514/1.6691.
11. Sullivan J, Grimberg S, D'Amico S. Comprehensive Survey and Assessment of Spacecraft Relative Motion Dynamics Models. *J Guid Control Dyn*. 2017;40(8):1837-1859. doi:10.2514/1.G002309.
12. Gim D-W, Alfriend KT. State Transition Matrix of Relative Motion for the Perturbed Noncircular Reference Orbit. *J Guid Control Dyn*. 2008. doi:10.2514/2.6924.
13. deBruijn F, Gill E, How J. Comparative analysis of Cartesian and curvilinear Clohessy-Wiltshire equations. *J*

Aerosp Eng Sci Appl. 2011;3(2):1-15. doi:10.7446/jaesa.0302.01.

14. Schaub H, Vadali SR, Junkins JL, Alfriend KT. Spacecraft Formation Flying Control using Mean Orbit Elements. *J Astronaut Sci*. 2000;48(1):69-87. doi:10.1016/S1000-9361(08)60069-2.
15. Demars KJ, Cheng Y, Jah MK. Collision Probability with Gaussian Mixture Orbit Uncertainty. *J Guid Control Dyn*. 2014;37(3). doi:10.2514/1.62308.
16. Vallado DA, Alfano S. Curvilinear coordinates for covariance and relative motion operations. *Adv Astronaut Sci*. 2012;142:929-946.
17. Yamanaka K, Ankersen F. New State Transition Matrix for Relative Motion on an Arbitrary Elliptical Orbit. *J Guid Control Dyn*. 2008;25(1):60-66. doi:10.2514/2.4875.
18. Schweighart SA, Sedwick RJ. High-Fidelity Linearized J Model for Satellite Formation Flight. *J Guid Control Dyn*. 2002. doi:10.2514/2.4986.
19. Gaias G, Ardaens JS, Montenbruck O. Model of J2 perturbed satellite relative motion with time-varying differential drag. *Celest Mech Dyn Astron*. 2015;123(4):411-433. doi:10.1007/s10569-015-9643-2.
20. Fehse W. Orbit dynamics and trajectory elements. In: *Automated Rendezvous and Docking of Spacecraft*. ; 2009:29-75. doi:10.1017/cbo9780511543388.004.
21. Fehse W. Approach safety and collision avoidance. In: *Automated Rendezvous and Docking of Spacecraft*. ; 2003:76-111. doi:10.1017/cbo9780511543388.005.
22. Chioma VJ, Titus NA. Expected Maneuver and Maneuver Covariance Models. *J Spacecr Rockets*. 2008;45(2):409-412. doi:10.2514/1.31154.
23. Tapley BD, Schutz BE, Born GH. Consider Covariance Analysis. In: *Statistical Orbit Determination*. ; 2004. doi:10.1016/B978-0-12-683630-1.X5019-X.
24. Wright JR. Orbit Determination Tool Kit Theory & Algorithms. 2013. http://help.agi.com/odtk/ODTK/pdf/MathSpec.pdf. Accessed November 14, 2017.
25. Kalman RE. A New Approach to Linear Filtering and Prediction Problems. *J Basic Eng*. 2011;82(1):35. doi:10.1115/1.3662552.
26. Sullivan J, D'Amico S. Nonlinear Kalman Filtering for Improved Angles-Only Navigation Using Relative Orbital Elements. *J Guid Control Dyn*. 2017. doi:10.2514/1.G002719.
27. Julier SJ, Uhlmann JK. New extension of the Kalman filter to nonlinear systems. In: *Proceedings of SPIE 3068Signal Processing, Sensor Fusion, and Target Recognition VI*. ; 1997:182. doi:10.1117/12.280797.
28. Carpenter JR. Non-Parametric Collision Probability for Low-Velocity Encounters. In: *17th AAS/AIAA Space Flight Mechanics Meeting*. Sedona, AZ; 2007:AAS 07-201. https://ntrs.nasa.gov/archive/nasa/casi.ntrs.nasa.gov/20070017983.pdf.
29. Chan KF. *Spacecraft Collision Probability*. The Aerospace Press; 2008.
30. Phillips MR. Spacecraft Collision Probability Estimation for Rendezvous and Proximity Operations. 2012. https://digitalcommons.usu.edu/etd/1398.
31. Patera RP. A general method for calculating satellite collision probability. *Adv Astronaut Sci*. 2000;105 II(4):1275-1290. doi:10.2514/2.4771.
32. McKinley D. Development of a Nonlinear Probability of Collision Tool for the Earth Observing System. In: *AIAA/AAS Astrodynamics Specialist Conference*. ; 2012:1-16. doi:10.2514/6.2006-6295.
33. Lovell TA, Tragesser S. Guidance for Relative Motion of Low Earth Orbit Spacecraft Based on Relative Orbit Elements. In: *AIAA/AAS Astrodynamics Specialist Conference*. ; 2004:1-16. doi:10.2514/6.2004-4988.
34. Mahalanobis PC. On the Generalized Distance in Statistics. *Proc Natl Inst Sci India*. 1936;2(1):49-55.